Journal of Structural Geology 32 (2010) 878–885

Contents lists available at ScienceDirect

Journal of Structural Geology

journal homepage: www.elsevier.com/locate/jsg

Determination of geometric parameters of fracture networks using 1D data

Tivadar M. Tóth*

Department of Mineralogy, Geochemistry and Petrology, University of Szeged, P.O. Box 651, H-6701 Szeged, Hungary

ARTICLE INFO

Article history:
Received 25 February 2008
Received in revised form
13 April 2009
Accepted 19 April 2009
Available online 3 May 2009

Keywords:
Fracture network simulation
Scanline
Length exponent
Fractal geometry

ABSTRACT

To simulate a suitable fracture network for hydrogeological modelling, input statistical data of the individual faults, as well as fracture sets, should be determined first using either 2D sections or 1D scanlines. Although the accuracy of this measurement is fundamental, exact determination is rather problematic and is usually possible only at a particular scale. This paper introduces a coupled method for computing length exponent (E) and spatial density (D^c), the two most essential parameters for modelling fracture networks. To calculate the length exponent, data sets of at least two independent imaging processes are needed. Utilizing different sensitivity thresholds of the two methods and the well-known analytical form of a fracture length distribution function, its parameters can be calculated. To estimate the spatial density of fracture centres in 3D, the series of intersections should be analysed as a fractional Brownian motion and then calibrated with virtual wells simulated with optional modelling software. The method makes fracture intensity logging possible along scanlines. Based on these approaches, there is no need to import fracture parameters from the outcrop survey or from other parts of the reservoir, because all geometric information of the fracture system refers to the rock body under examination. Using site-specific parameters makes fracture network modelling more reliable.

1. Introduction

Under appropriate physical conditions, rock deformation produces brittle structures. Since the resulting fracture system has an essential role in the hydraulic behaviour of the rock body, reconstructions of both the structural evolution and the spatial appearance of the fracture network are crucial. Faults regularly appear at different scales, from the submicroscopic size to the kilometre scale (Allègre et al., 1982; Turcotte, 1992; Ouillon et al., 1996) with structural and geometric features comparable at all magnitudes (Korvin, 1992; Turcotte, 1992; Long, 1996; Weiss, 2001). Such behaviour ensures the theoretical background of fracture network modelling concept, in which structural data measured at micro- or meso-scales are used to upscale information to larger dimensions. Mathematical simulation of a 3D fracture network at the reservoir scale, taking into account also the lithological and structural setting, is especially important because hydraulically active fracture sets are usually out of the scale of both microstuctural and seismic measurements (Paillet et al., 1993; Childs et al., 1997).

Simulation generally has two sequential steps. At the first point, geometric parameters of the individual faults, as well as fracture sets, must be determined. These parameters should serve the firm base for the simulation itself using appropriate modelling software. In the last decades, numerous algorithms and programs have been developed (for example Long (1996), Zhang and Sanderson (2002), FracMan (Dershowitz et al., 1993), FracNet (Gringarten, 1998), RepSim (Tóth et al., 2004) etc.) to solve diverse problems regarding fractured reservoirs. Whilst the exact spatial definition of hydraulically active faults is desirable, this is not generally possible and so in most cases a simulated network is used for hydrogeological assessment. That is why most approaches aim to generate a stochastic reconstruction of a network of individual fractures (discrete fracture network—DFN methods). To do so, in addition to structural parameters (e.g. fault generations, kinematic indicators, fracture filling mineral paragenesis) additional geometric parameters of the fault set, such as length, aperture, orientation and spatial density, are required. Although accuracy of determination of these parameters is fundamental to the success of modelling, measurements are rather problematic (Yang et al., 2004) and are usually possible exclusively at a particular scale (La Pointe and Hermanson, 2001; Zimmermann et al., 2003). Besides using outcrops, geological cross-sections, borecores or thin sections for measurement on 2D sections, parameter estimation is mainly possible along 1D scanlines (Priest and Hudson, 1981; La Pointe and Hermanson, 2001; Priest, 2004 and references therein), supplied by well-logs.

* Tel.: +36 62 544640. fax: +36 62 426459.
E-mail address: mtoth@geo.u-szeged.hu

0191-8141/$ – see front matter © 2009 Elsevier Ltd. All rights reserved.
doi:10.1016/j.jsg.2009.04.006

The aim of the present paper is to introduce novel algorithms for determining fracture length distribution and spatial density using 1D datasets. Since density can be defined in several different ways (e.g. Long, 1996), the estimation methods should be harmonized with the modelling system as well.

2. Geometric parameters of fracture systems

In addition to structural data, quantitative parameters also play an essential role in describing fracture systems. A single fracture is usually a finite, complexly buckled 2D surface that can be approximated by planes (Chiles and de Marsily, 1993). In a homogeneous, isotropic rock body under pure tensile stress, the shape of a fracture is close to circular (Twiss and Moores, 1992); whereas in the case of stratified sedimentary rocks, a more anisotropic appearance (ellipse) is more common. However, the shape of fracture planes may be extremely complex due to overlapping structural effects; in order to make the simulated fracture network appropriate for hydrodynamic modelling, some limitations must be used. Since flow between smooth, parallel plates is the only fracture geometry that is amenable to exact treatment for hydrodynamic modelling (Witherspoon et al., 1980; Neuzil and Tracy, 1981; Zimmerman and Bodvarsson, 1996), fractures should be approximated by thin discs. And while the most regularly followed choice for fracture shape under these constraints is a circle (“penny-shaped”), other approximation estimates also occur. In what follows, fractures are modelled by penny-shaped cracks by taking into account that many other simulators (e.g. FracMan, Dershowitz et al., 1993) use synthetic faults of a polygonal shape. A circle in 3D is explicitly defined through the co-ordinates of the centre, the radius and orientation. In the case of fault systems the spatial function of the geometric centres, as well as the distribution functions of length, strike and dip must be determined. Because hydraulic characterization of fracture networks presumes a positive volume of each fracture, circles are usually replaced by discs with a certain aperture (”parallel plate model”, Witherspoon et al., 1980). Symbols that will be used through the modelling process are collected in Table 1.

One of the most important parameters concerning fluid migration through fracture networks is the size (diameter) of the fractures. Davy (1993), Bour and Davy (1997), de Dreuzy et al. (2001), Bonnet et al. (2001), among many others, inferred an asymmetric length distribution of fracture diameter, which, according to the most widely used model (e.g. Yielding et al., 1992; Min et al., 2004) follows the

Table 1
Symbols used in the text.

Variable	Explanation of the variable
L	Diameter of a penny-shaped fracture
D	Fractal dimension in general
D_1, D_2, D_3	Fractal dimensions of the fracture network traces in 1D, 2D, 3D Euclidean spaces
D_2^c	Fractal dimension of fracture centres of a 2D network trace
D_3^c	Fractal dimension of fracture centres in 3D
E, F	Parameters of the length distribution function
E	Length exponent
A, B	Parameters of the aperture function
L_1, L_2	Detection length thresholds of different fracture identification methods
a_1, a_2	Detection aperture thresholds of different fracture identification methods
α	Dip of a fracture
β	Strike of a fracture
r	Size of a box in the box-counting algorithm
H	Hurst exponent
$f(n)$	Series of fracture intersection depths
w	Length of an interval used for the R/S analysis

$$N(L) = F^*L^{-E} \tag{1}$$

power law function, where $N(L)$ is the number of fractures with a diameter of L; E and F are the parameters of the fracture length distribution function.

Aperture becomes essential only if the simulated fracture network is evaluated hydrogeologically, i.e. it is used for estimating porosity and permeability tensor. Exact determination of aperture is quite problematic (Vermilye and Scholz, 1995). The original aperture can be significantly modified due to water-rock interaction processes, either solution or precipitation. Aperture distribution also depends considerably on the orientation of the current in situ stress field (Allen and Roberts, 1982), which makes its measurement rather uncertain. Moreover, fluid migration in a crack is also a function of the roughness of the fracture wall (Kumar and Bodvarsson, 1990; Kumar et al., 1991; Liu, 2005), which further complicates the estimation of the effective aperture values. To solve this problem, Leckenby et al. (2005) suggest measuring the thickness of entirely cemented fractures as “paleo-apertures”; whereas Keller (1998) uses computer tomography for the same purpose. Even if the measurement is uncertain, aperture, like fracture length, seems to follow a power law distribution function (de Dreuzy et al., 2002; Ortega et al., 2006). Furthermore, between these two parameters, a tight linear correlation can be assumed, one that is based both on theoretical (Pollard and Segall, 1987) and empirical (Barton and Larsen, 1985; Loiseau, 1987; Vermilye and Scholz, 1995; Gudmundsson, 2000; Gudmundsson et al., 2001) results. Specifically,

$$a = A^*L + B \tag{2}$$

where A and B are the parameters of the aperture function. In natural cases $B \neq 0$ values must be an error caused by inadequate regression analysis and should not be used for modelling. The ratio of maximal aperture and length (i.e. the slope of the linear function in (2)) varies around 2×10^{-3}–8×10^{-3} for joints and 3×10^{-3}–3×10^{-2} for faults in the case of many different rock types (Opheim and Gudmundsson, 1989; Vermilye and Scholz, 1995).

While definitions of fracture diameter and aperture are relatively straightforward, there are plenty of approaches to define the spatial density of fracture networks. Among these are included fracture intensity, fracture density, fracture index, fracture surface area, fracture intersection density and fracture spacing. Detailed measurements by many authors (Barton and Larsen, 1985; La Pointe, 1988; Hirata, 1989; Matsumoto et al., 1992; Kranz, 1994; Tsuchiya and Nakatsuka, 1995; Roberts et al., 1998) evidence that fracture networks usually exhibit fractal-like geometry independent of lithology and structural evolution. This means that not only the length and aperture data of fractures, but also their spatial distribution depends on the scale of measurement. Accordingly, fractured reservoirs can be determined by more and less closely fractured zones juxtaposed at each scale; and so an adequate measure for spatial density of fracture centres is their fractal dimension. A common way to calculate fractal dimension is the widely used box-counting method (Mandelbrot, 1983, 1985; Barton and Larsen, 1985; Barton, 1995), in which

$$N(r) \sim r^{-D} \tag{3}$$

The number of boxes ($N(r)$) necessary to cover the fracture pattern is proportional to the size of these boxes (r).

However, for successful modelling in 3D, the fractal dimension of the cloud of fracture centres embedded in 3D Euclidean space

is needed; this parameter is rather hard to measure and can only be estimated. Because of structural geological reasons a fault network usually consists of sets of sub-parallel fractures. In a theoretical case of parallel fractures, the centres of their traces on any 2D plain are the projections of the original 3D pattern of centres onto the plane in question. In this case, following the simple theorem of fractal geometry concerning the dimension of the projection:

$$D_2^c = \min(D_3^c,\ 2) \tag{4}$$

$D_2^c = D_3^c$ follows as long as $D_3^c < 2$. Finally, in a real case, D_3^c used for modelling is defined as an average of D_2^c data determined on several planes (Tóth et al., 2004).

3. The model used-RepSim

Accordingly, fracture networks can be described using fractal geometry in two respects. On one hand, length distribution follows the power law distribution; while on the other hand, fractures above any length threshold display a scale invariant pattern in 3D. The discrete fracture network modelling system, called RepSim (Tóth et al., 2004) is based on these assumptions, and follows the methodological steps:

1. The model region is divided into unit cubes of the homogenous parameter set. Each cell is characterized by D_3^c, E, F, A values and a set of (α, β) data pairs. These cubes appear as the generator elements of the following recursive algorithm.
2. Next, edges of the boxes are divided into $r(\in N)$, so that r^3 new cubes are formed.
3. From this set of smaller cubes, using the input fractal box dimension and based on the relation $N(r) = r^{-D}$, the number of boxes of edge length r that contain fracture seeds can be calculated. The filled boxes themselves are selected at random afterwards.
4. Division and selection of new sets of smaller cubes are repeated in a recursive manner; while, in the final step, the centre points of the last set of cubes are chosen as seed points. As the boxes become smaller, the number of filled boxes increases similar to the box-counting method.

Because of the recursive nature of the algorithm and the use of the resolved box dimension, the final aggregate of points is a fractal of the same measure (D^c_3). The points are finally used as seeds for the penny-shaped fractures with random diameter, strike and dip values of the measured distributions. Since fracture aperture is only related to the hydraulic conductivity and does not influence the network geometry, aperture is calculated for each fracture using the A parameter and equation (2).

4. Determination of geometric parameters of fractures

Fractures can be considered as 2D objects embedded in a 3D volume. Exact measurement of their geometric parameters is possible for small scale samples by diverse techniques (Hellmuth et al., 1993; Montemagno and Pyrak-Nolte, 1995; Frieg et al., 1998; Wildenschild et al., 2002; McDermott et al., 2003; Onishi and Shimizu, 2003); however, above very small scales it becomes more difficult. Traces of fault systems can generally be measured on different 2D sections (e.g. Zhang and Einstein, 1998), such as aerial photos (e.g. Clifton and Schlische, 2003), outcrops, hand specimens or microscopy via fluid-inclusion planes or cement filled micro-fractures (Gomez and Laubach, 2006). Another way is using 1D sections (scanlines) at diverse scales (e.g. La Pointe and Hermanson, 2001). Evaluation of the 2D network of fracture traces is an image analysis problem (Gomez and Laubach, 2006); hereafter, only assessments of 1D sections are focused on.

4.1. Evaluation of 1D sections

4.1.1. Estimation of fractal dimension (D_3^c)

Well-log methods are often used to study fractured reservoirs (Bean, 1996; Marsan and Bean, 1999; Liu, 2006). Borehole image logs (e.g. BHTV—Borehole Televiewer) and diverse core imaging processes, result in deterministic data sets of fractures with exact spatial position (Tezuka and Watanabe, 2000; Yang et al., 2004). The series of intersection points between the fracture network and the borehole can further be analyzed as a point process. As has been shown previously, above any length (or identically, aperture) threshold, fractures define a scale invariant pattern in 3D. Since all the above geophysical methods have their own sensitivity limits, the series of fracture intersection points must have the same feature, so it must be a fractal too. Fractal objects of this kind (fractal time series) are widespread in geological and geophysical literature; change of Earth's magnetic field in space and time (e.g. Smirnova et al., 2001; Wanliss and Cersosimo, 2006), seismic noise (Turcotte, 1992) or even mineral zoning (Bryxina et al., 2002) can be modelled using self-similar and self-affine fractal time series. Typical examples of statistically self-affine fractals are fractional Brownian motions (*fBm*). Increments of an *fBm* with parameter H (Hurst exponent) are stationary and self-affine with a fractal dimension of $D = 2 - H$. On this basis, the point process that describes fracture depth series is a self-affine fractal, which can be studied as a *fBm*.

There are several methods to determine the Hurst exponent (Hurst, 1951) of a *fBm*. Among them, the most popular approaches are the R/S (rescaled range), the R/L (roughness/length) analysis, spectral analysis or variography, each of which aims to estimate H, although the numerical result of the diverse methods may be significantly different (Malamud and Turcotte, 1999; Arizabalo et al., 2004). Based on our numerical experiments, as well as the results of Cimino et al. (1999) and Telesca et al. (2004), we use R/S analysis to estimate the Hurst exponent of a fracture intersection point series. For a given $f(n)$ point process (series of fracture intersection depths in the present case), the algorithm applied follows these steps (Telesca et al., 2004):

1. The linear trend is subtracted from $f(n)$;
2. For any interval w, $R(w) = f(n)_{\max} - f(n)_{\min}$ (the range);
3. For the same interval, $S(w)$ is defined as the standard deviation of $(f(n) - f(n-1))$;
4. Let us define $R/S(w) = M(R(w)/S(w))$ with M as a mean value (R/S is the rescaled range);
5. If the signal is fractional Brownian motion, it exhibits power-law scaling so that $R/S(w) = w^H$, where from H can be estimated.

While such calculation leads to a proper fractal dimension of the fracture intersection pattern along any scanline, there is no reason to suppose a constant spatial density with depth. That is why dimension should be logged so that each depth interval is characterized by its own H value. The limit for dimension logging is defined by the numerical experiments of Katsev and L'Heureux (2004), who infer that R/S analysis is rather uncertain for short series and suggest using at least 400-500 points (fractures) for a reliable result.

4.1.2. Determination of length exponent (E)

Because the orientation and the depth dependent fractal dimension are determined using well-log data, they are both

fundamental site-specific parameters. However, the length exponent is also essential in modelling; Yang et al. (2004) suggest that fracture length cannot be determined directly and should instead be obtained from an outcrop survey. Recently, Priest (2004) introduced a numerical method to the calculate fracture size distribution using scanline data. Mauldon and Derschowitz (in press) alternatively suggest an indirect approach to deduce the size distribution using measured transmissivity behaviour. While the exact position of the fractures that intersect the well can be detected by well-log data, their size is difficult to document, because most fractures crosscut the mantle of the core. As a consequence, length distribution is considered to be the most uncertain of the parameters related to hydraulic conductivity.

While diverse borehole imaging geophysical methods detect fractures in similar scale intervals, they all have slightly different sensitivity; each method with its own detection limit. Consequently, fractures identified by a less sensitive method must constitute a subset of those discovered by the other one. The difference is the set of fractures between the two detection limits. It becomes clear when distinguishing fracture density logs of the same well detected by two different well-log methods, BHTV and core imaging, respectively (Fig. 1). In this example, core imaging systematically identifies more fractures with a constant difference ($\Delta N(L)$) along the whole well.

Keeping such a difference, as well as the detection limits characteristic for the applied methods (L_1, L_2), parameters of the fracture length distribution function ($N(L) = F^* L^{-E}$, e.g. Segall and Pollard, 1983; Heffer and Bevan, 1992) can be calculated (Fig. 2) using

$$N(L_1) = F^* L_1^{-E} \tag{5}$$

$$N(L_2) = F^* L_2^{-E} \tag{6}$$

and consequently

$$\frac{N(L_1)}{N(L_2)} = \left(\frac{L_1}{L_2}\right)^{-E} \tag{7}$$

where from

$$\frac{\log(N(L_1)) - \log(N(L_2))}{\log(L_1) - \log(L_2)} = -E \tag{8}$$

and afterwards F obviously comes from (5).

While the detection limit usually is defined as an aperture value (a_1, a_2), it is a linear function of length (Loiseau, 1987; Vermilye and Scholz, 1995; Gudmundsson, 2000; Gudmundsson et al., 2001) and so

$$\frac{a_1}{a_2} = \frac{A^* L_1}{A^* L_2} = \frac{L_1}{L_2}$$

in (7).

Accordingly, having data of two independent well-log measurements, length distribution can be computed by the following algorithm:

1. The well is subdivided into intervals for which fracture density is calculated for both methods (in m^{-1});
2. The difference of these density values ($\Delta N(L)$) is the parameter proportional to the length exponent;
3. Using equations (5)–(8), E and F parameters can be computed for each interval with homogenous $\Delta N(L)$;

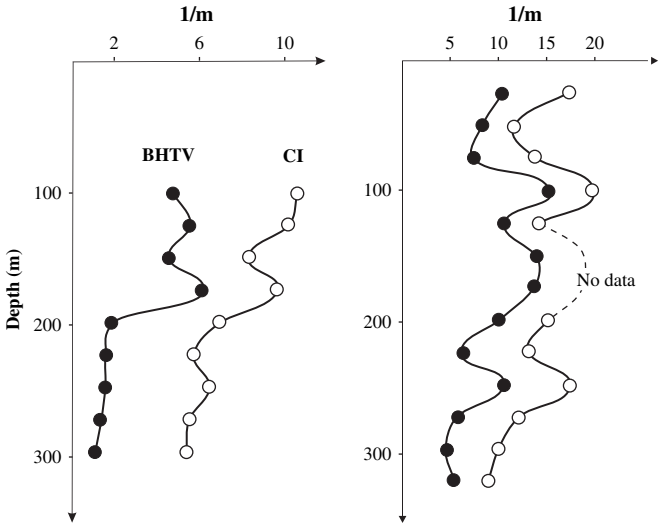

Fig. 1. Fracture density logs for two selected wells detected by two different well-log methods, BHTV and core imaging, CI), respectively.

4. Prior to calculations, the detection limit, as a function of the aperture, should be determined for each well-log method.

5. Case study—Mórágy granite body

The above techniques are introduced in the case of the Mórágy granite body, which is the host rock of the radioactive waste disposal in Hungary (Balla, 2003). A significant part of the Carboniferous intrusion (Buda et al., 1999; Klötzli et al., 2004) is covered by young sediments, and only a small portion of it is available for outcrop survey. Petrographically, the igneous body is composed of diverse granitoid subtypes, such as monzonite and monzogranite, which, due to a polymetamorphic evolution under greenschist facies conditions, exhibit a slightly foliated structure (Király and Koroknai, 2004). During the subsequent post-metamorphic deformation events, a mutual fracture network developed. Based on evaluation of the BHTV data of over 60,000 single fractures representing 20 wells, two main groups of faults can be

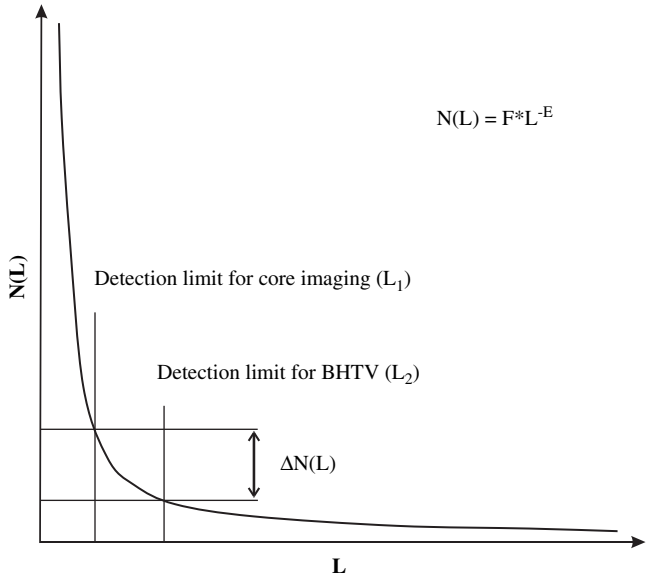

Fig. 2. Calculation of length exponent, E, using $\Delta N(L)$ value and the detection limits characteristic for the applied imaging methods, L_1, L_2).

emphasized. One cluster shows very high dips (70°–80°), with a NW–SE strike; whilst another shows a strike of ENE–WSW and a similar dip (Maros et al., 2004). Most veins are filled in by a complex sequence of common hydrothermal minerals (calcite, dolomite, clay minerals, quartz and chlorites; Kovács-Pálffy and Földvári, 2004). In places phases of a late-magmatic, hydrothermal assemblage (gold, stibnite, barite among others; Gatter and Török, 2004) occur.

5.1. 2D Sections

To estimate fracture parameters of the Mórágy granite, 1D and 2D sections of different scales were used. 2D measurements were acquired by evaluating digital images of the granite wall at the village Erdősmecske (Fig. 3). Three differing scales were analysed; in addition to the sub-vertical wall (roughly 10 × 60 m in area), we used 5 × 10 m-sized portions of the wall as well as hand-collected specimens around 20 × 20 × 20 cm in size.

On the wall, ~6500 individual fractures were digitized. Trace length distribution follows the theoretically valid power law behaviour with $E = 2.48$. At extreme lengths, a significant misfit is obvious (Fig. 4), emphasizing that detection is rather uncertain close to the two limits. Similar histograms and length exponent values can be obtained for the other scales; for segments of the wall, $E = 2.46 \pm 0.2$; whereas for the hand-collected specimens, $E = 2.36 \pm 0.06$ (Kaszai, 2003). Consequently, except for errors due to uncertain detection and representativity mistakes at extreme lower and upper values, trace length distribution follows a power law with similar parameters and can be computed for each scale. Also a linear relationship between length and aperture can be inferred using measurements on the hand-collected specimens. The slope of the regression line in (2) is $A = 2.7 \times 10^{-2}$, a number that is within the interval typical for faults for different rock types (Opheim and Gudmundsson, 1989; Vermilye and Scholz, 1995).

The fractal dimension values are $D_2 = 1.47 \pm 0.07$ for the 12 segments shown in Fig. 4, While for fracture centres $D_2^c = 1.56$. In the case of the whole wall, $D_2^c = 1.56 \pm 0.07$ for the segments and $D_2^c = 1.45 \pm 0.06$ for hand-collected specimens (Fig. 5).

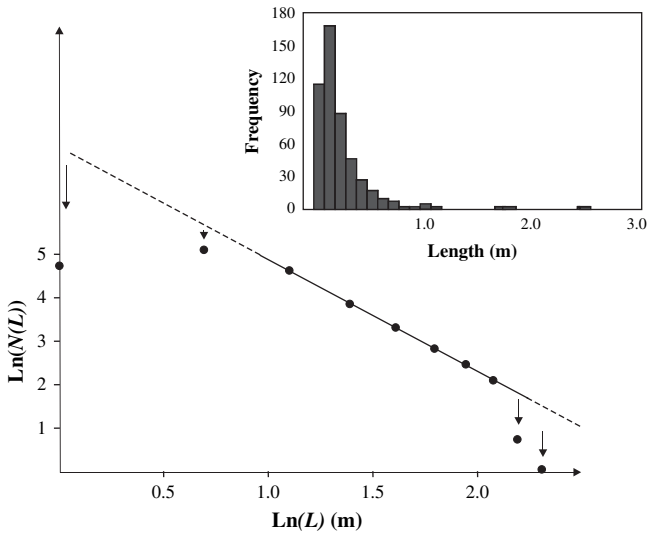

Fig. 4. Fracture length distribution for the Erdősmecske granite wall at meso-scale. Misfit is caused by diminishing detection for small values and censoring at large values. Inset: Histogram of fracture lengths prior to logarithmic transformation.

5.2. 1D Sections

For 1D sections, BHTV (Borehole Televiewer) and Core Image (CI) data are used, representing a borecore that penetrated the Mórágy granite complex to a 400 m depth. The core imager device was developed by the Geological Institute of Hungary for high-quality resolution optical scanning of borecores (Maros and Pásztor, 2001). The two imaging processes result in a continuous spectrum for the same fracture systems with significantly different sensitivity. They satisfy the assumptions of the above introduced 1D

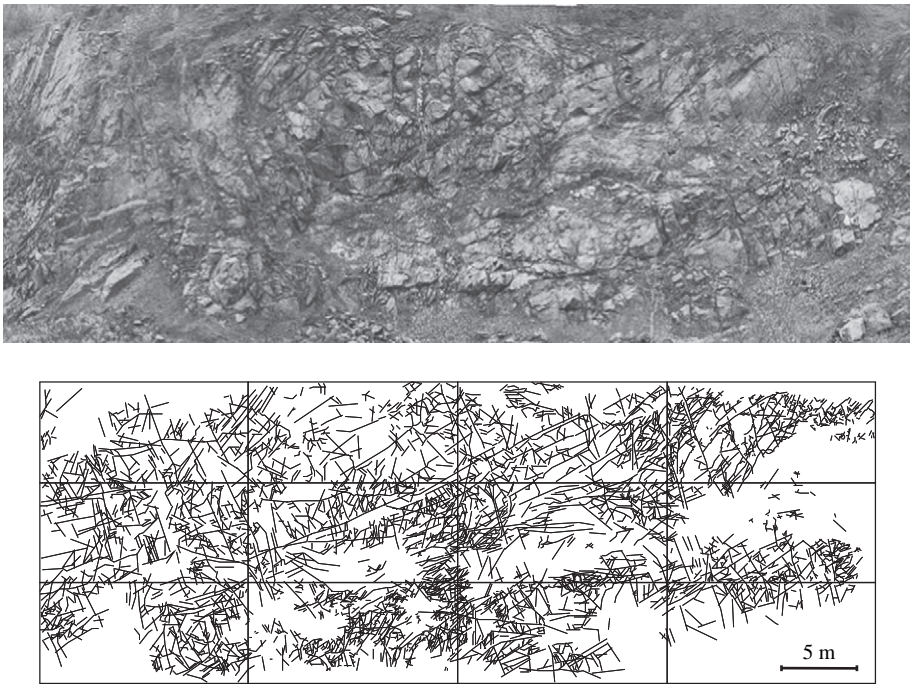

Fig. 3. (a) The granite wall at Erdősmecske. (b) Digitized fracture network of the wall.

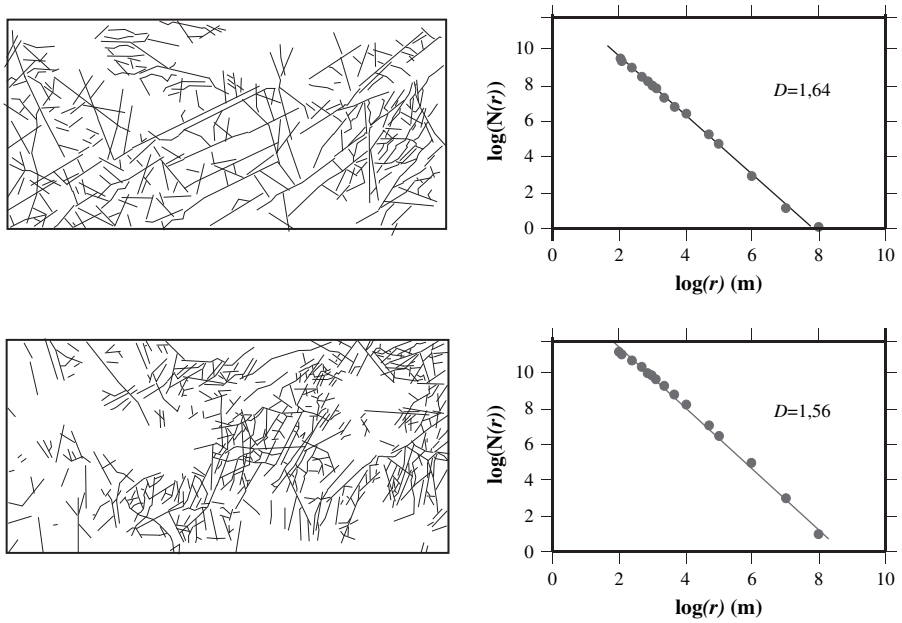

Fig. 5. Examples for spatial density calculations via the box counting method for the studied granite wall at meso- and micro-scales.

calculations. Sensitivity thresholds for the two methods are 500 μm for Core Imaging and 750 μm for BHTV, respectively. Consequently, H and $\Delta N(L)$ can be computed along the well.

For calculations, the well was subdivided into 25 m-long intervals, each of which consisted of at least 500 fractures, a number sufficient to estimate a reliable Hurst exponent (Katsev and L'Heureux, 2004). The CI can detect many more fractures than the BHTV can; in fact $\Delta N(L) = 550$ for the whole well. Furthermore, variation of $\Delta N(L)$ is rather stable along the core (see Fig. 1b) except for the middle sector, where CI data are unreliable. Consequently, the whole well can be characterized by a single E value. However, the estimated number (1.41) is much lower than that measured on different 2D sections in another part of the granitoid body, in the case of different wells in the region E varies between 1.08 and 2.64 (Tóth, 2004), suggesting a highly heterogeneous internal structure.

In order to calibrate the relationship between the Hurst exponent and the fractal dimension of the fracture centres in 3D (i.e. the $H = f(D_3^c)$ function), a series of fracture networks was simulated with $D_3^c = 1.1, 1.3, 1.5, 1.7$, using the RepSim code. Strike and dip data are from BHTV measurements and $E = 1.41$. Each simulated network was crosscut by a virtual well in order to obtain a series of fracture intersections of at least 1000 points (Fig. 6). R/S analysis was used to compute H for each series. Calculations were completed for 5 series of each of 100-, 200-, 300- and 400-point-long segments to compute averages and standard deviation values for each case. We found that averages of H converged, while standard deviations decrease rather quickly when an increasing number of points involved in the R/S analysis. For all $D_3^c = 1.1, 1.3, 1.5, 1.7$ cases, variation coefficient $\sigma/M < 0.05$ if at least 400 points are used (Fig. 7). Based on the H values calculated using these 400-point-long series, a simple linear calibration results in a $D_3^c = 2.63{*}H - 0.21$ equation with a high correlation coefficient ($\rho = 0.99$). Based on this relationship, D_3^c varies between 1.39 and 1.79 along the studied well, values comparable to those obtained using the 2D measurements.

The fracture network model near the studied well clearly exhibits more and less fractured zones, pointing to the advantage of using adequate fracture parameters for each depth interval (Fig. 8).

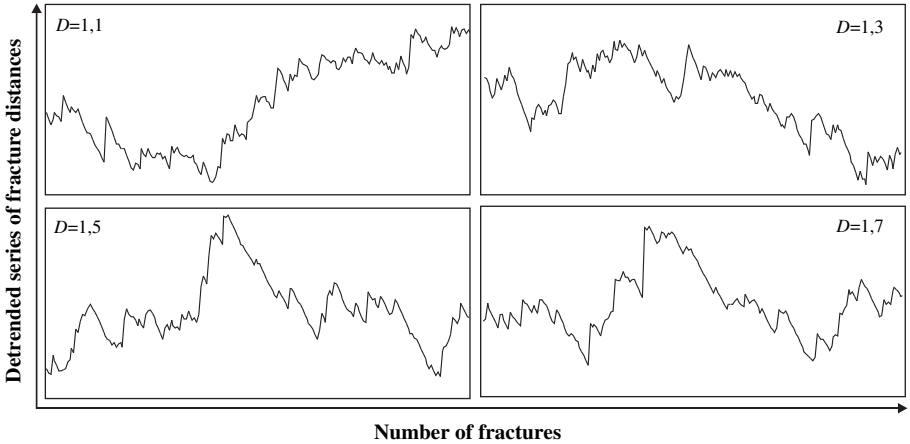

Fig. 6. Examples of detrended fracture density signals calculated by virtual wells cross-cut networks simulated using the RepSim code, $D^c = 1.1, 1.3, 1.5, 1.7$).

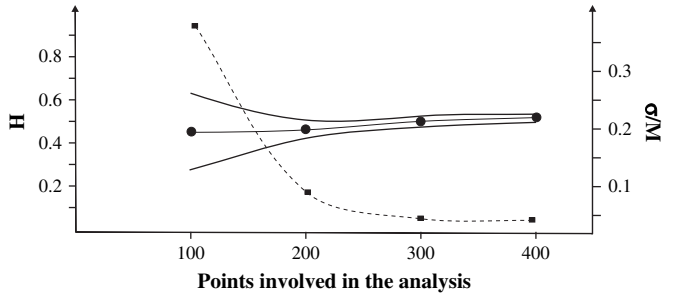

Fig. 7. Change of mean and standard deviation of the calculated Hurst exponent values as a function of points involved in the R/S analysis. Dashed line shows the decrease of variation coefficient, σ/M).

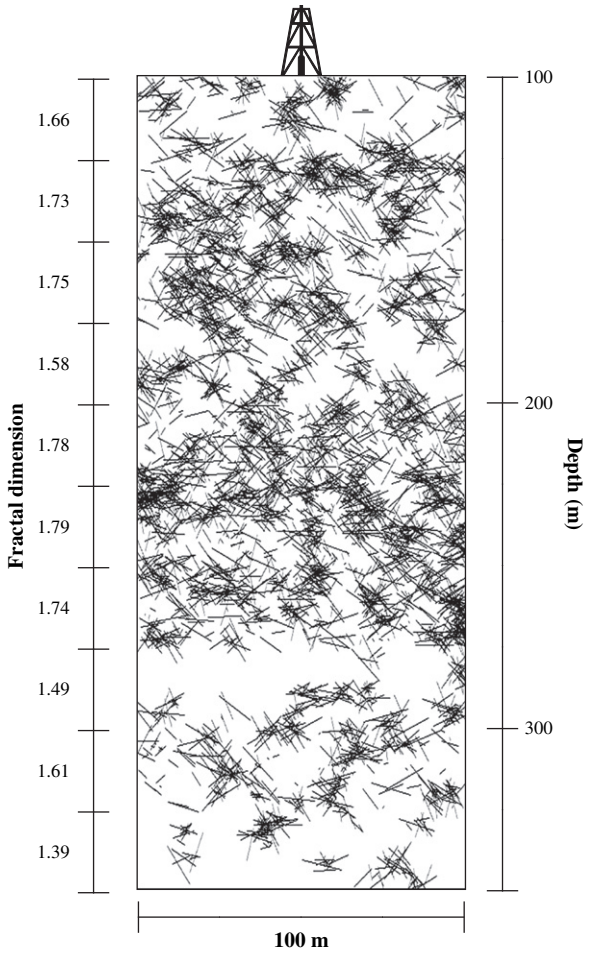

Fig. 8. Fracture network model near the studied well based on accurate parameters for each depth interval. Scale bar shows the appropriate D^c values for each 25 m interval.

6. Conclusions

Modelling fractured reservoirs underground is a huge challenge because of the difficulty of measuring model parameters. While strike and dip of individual fractures can obviously be obtained by evaluating BHTV or other imaging data, determination of the length exponent and spatial distribution of scale-dependent fracture systems has been a difficult problem.

This paper introduces a coupled method for computing E and D_3^c, the two most essential parameters in modelling fracture networks (Zhang and Sanderson, 2002). To calculate the length exponent, data sets of at least two independent imaging processes are required. Utilizing different sensitivity thresholds of the two methods, as well as the well-known analytical form of a fracture length distribution function, the required parameters can be calculated. To estimate the spatial density of fracture seeds, the series of intersections as a *fBm* should be analysed. Dimension logging is a rather sensitive way to follow the variability of fracture intensity with depth. Because coefficients of the $H = f(D_3^c)$ linear function may differ well by well, or even interval by interval in the same well, using the above method for calibration makes estimation of modelling parameters quite flexible. There is no need to import parameters from another parts of the reservoir; all information (E, F, D_3^c, α, β) concerns the rock body under examination. Using only site-specific parameters makes fracture network modelling more reliable.

Acknowledgements

RHK is kindly thanked for supporting BHTV and CI data. The project was financially supported by the RHK Kht., the OTKA Foundation (No. K60768) and the NKTH (No. RET-07/2005). Comments of Andres Perez-Estaun and an anonymous reviewer improved the manuscript significantly. English was corrected by the American Journal Experts.

References

Allègre, C.J., Le Mouel, J.L., Provost, A., 1982. Scaling rules in rock fracture and possible implications for earthquake prediction. Nature 297, 47–49.
Allen, T.O., Roberts, A.P., 1982. Production Operations. Oil and Gas Consultants International, Inc., Tulsa. 113–169.
Arizabalo, R.D., Oleschko, K., Korvin, G., Ronquillo, G., Cedillo-Pardo, E., 2004. Fractal and cumulative trace analysis of wire-line logs from a well in a naturally fractured limestone reservoir in the Gulf of Mexico. Geofísica Internacional 43 (3), 467–476.
Balla, Z., 2003. General characteristics of the Bátaapáti, Üveghuta) Site, South-western Hungary. Annual Report of the Geological Institute of Hungary 2003, 73–86.
Barton, C.C., 1995. Fractal analysis of scaling and spatial clustering of fractures. In: Barton, C.C., La Pointe, P.R. (Eds.), Fractals in the Earth Sciences. Plenum Press, New York, 168 pp.
Barton, C.C., Larsen, E., 1985. Fractal geometry of two-dimensional fracture networks at Yucca Mountain, Southwestern Nevada. In: Stephanson, O. (Ed.), Proceedings of International Symposium on Fundamentals of Rock Joints, pp. 77–84.
Bean, C.J., 1996. On the cause of 1/f-power spectral scaling in borehole sonic logs. Geophysical Research Letters 23, 3119–3122.
Bonnet, E., Bour, O., Odling, N.E., Davy, P., Main, I., Cowie, P., Berkowitz, B., 2001. Scaling of fracture systems in geological media. Reviews of Geophysics 39 (3), 347–383.
Bour, O., Davy, P., 1997. Connectivity of random fault networks following a power law fault length distribution. Water Resources Research 33, 1567–1583.
Bryxina, N.A., Halden, N.M., Ripinen, O.I., 2002. Oscillatory zoning in an agate from Kazakhstan: Autocorrelation functions and fractal statistics of trace element distributions. Mathematical Geology 34 (8), 915–927.
Buda, Gy., Lovas, Gy., Klötzli, U., Cousen, B.I., 1999. Variscan granitoids of the Mórágy Hills, South Hungary. Beihefte zur European Journal of Mineralogy 11 (2), 21–32.
Childs, C., Walsh, J.J., Watterson, J., 1997. Complexity in fault zone structure and implication for fault seal prediction. In: Moller-Pedersen, P., Koestler, A.G. (Eds.), Hydrocarbon Seals. Elsevier.
Chiles, J., de Marsily, G., 1993. Models of Fracture Systems. In: Bear, J., Tsang, C.F., de Marsily, G. (Eds.), Flow and Contaminant Transport in Fractured Rock. Academic Press.
Cimino, G., Del Duce, G., Kadonaga, L.K., Rotundo, G., Sisani, A., Stabile, G., Tirozzi, B., Whiticar, M., 1999. Time series analysis of geological data. Chemical Geology 161, 253–270.
Clifton, A.E., Schlische, R.W., 2003. Fracture populations on the Reykjanes Peninsula, Iceland: Comparison with experimental clay models of oblique rifting. Journal of Geophysical Research 108 (B2), 2074.
Davy, P., 1993. On the frequency-length distribution of the San Andreas fault system. Journal of Geophysical Research 98 12414–12151.
de Dreuzy, J.R., Davy, P., Bour, O., 2001. Hydraulic properties of two-dimensional random fracture networks following a power law length distribution 1. Effective connectivity. Water Resources Research 37 (8), 2065–2078.
de Dreuzy, J.R., Davy, P., Bour, O., 2002. Hydraulic properties of two-dimensional random fracture networks following power law distributions of length and aperture. Water Resources Research 38 (12), 121–129.
Dershowitz, W.S., Lee, G., Geier, J., Hitchcock, S., La Pointe, P., 1993. FracMan User Documentation. Golder Associates Inc., Seattle WA.
Frieg, B., Alexander, W.R., Bühler, C., Haag, P., Möri, A., Ota, K., 1998. In situ resin impregnation for investigating radionuclide retardation in fractured repository host rocks. Journal of Contaminant Hydrology 35, 115–130.

Gatter, I., Török, K., 2004. Mineralogical notes and fluid inclusion studies on quartz-feldspar granite pegmatites and quartz veins from Mórágy and Erdösmecske granitoid, S-Hungary. Acta Mineralogica-Petrographica Szeged 45 (1), 39–48.
Gomez, L.A., Laubach, S.E., 2006. Rapid digital quantification of microfracture populations. Journal of Structural Geology 28, 408–420.
Gringarten, E., 1998. FRACNET: Stochastic simulation of fractures in layered systems. Computers and Geosciences 24 (8), 729–736.
Gudmundsson, A., 2000. Fracture dimensions, displacements and fluid transport. Journal of Structural Geology 22 (9), 1221–1231.
Gudmundsson, A., Berg, S.S., Lyslo, K.B., Skurtveit, E., 2001. Fracture networks and fluid transport in active fault zones. Journal of Structural Geology 23 (2-3), 343–353.
Heffer, K.J., Bevan, T.G., 1992. Scaling relationships in natural fractures: Data, theory and application. SPE 20981, 367–376.
Hellmuth, K.H., Siitari-Kauppi, M., Lindberg, A., 1993. Study of porosity and migration pathways in crystalline rock by impregnation with 14C-poly-methylmethacrylate. Journal of Contaminant Hydrology 13, 403–418.
Hirata, T., 1989. Fractal dimension of fault system in Japan: fracture structure in rock fracture geometry at various scales. Pure and Applied Geophysics 131, 157–170.
Hurst, H.E., 1951. Long-term capacity of reservoirs. Transactions of the American Society of Civil Engineers 116, 770–808.
Kaszai, B., 2003. A Mórágyi gránit repedezettsége az erdösmecskei bánya területén., Brittle deformation of Mórágy granite around Erdösmecske., in Hungarian). MSc thesis, University of Szeged, Dept. Mineralogy, Geochemistry and Petrology, 52 pp.
Katsev, S., L'Heureux, I., 2004. Are Hurst exponents estimated from short or irregular time series meaningful? Computers and Geosciences 29 (9), 1085–1089.
Keller, A., 1998. High resolution, non-destructive measurement and characterization of fracture apertures. International Journal of Rock Mechanics and Mining Science 35 (8), 1037–1050.
Király, E., Koroknai, B., 2004. The magmatic and metamorphic evolution of the north-eastern part of the Mórágy Block. Annual Report of the Geological Institute of Hungary 2003, 299–310.
Klötzli, U.S., Buda, G., Skiöld, T., 2004. Zircon typology, geochronology and whole rock Sr-Nd isotope systematics of the Mecsek Mountain granitoids in the Tisia Terrane, Hungary. Mineralogy and Petrology 81, 1–2. 113-134.
Korvin, G., 1992. Fractal Models in the Earth Sciences. Elsevier, 396 pp.
Kovács-Pálffy, P., Földvári, M., 2004. Hydrothermal minerals and features in the Mórágy Granite Formation. 2003. Annual Report of the Geological Institute of Hungary, 319–333.
Kranz, R.L., 1994. Fractal point patterns and fractal fracture traces. In: Nelson, P.P., Laubach, S.E. (Eds.), Rock Mechanics. Balkema, Rotterdam, pp. 793–800.
Kumar, S., Bodvarsson, G.S., 1990. Fractal study and simulation of fracture roughness. Geophysical Research Letters 17, 701–704.
Kumar, S., Bodvarsson, G.S., Boernge, J., 1991. Fractal characteristics of fracture roughness and aperture data. High-Level Nuclear Waste Management, Proceedings of the Second International Conference, Las Vegas, Nevada, pp. 279-284.
La Pointe, P.R., 1988. A method to characterize fracture density and connectivity through fractal geometry. International Journal of Rock Mechanics and Mining Science & Geomechics Abstracts 25, 421–429.
La Pointe, P.R., Hermanson, J., 2001. 3-D reservoir and stochastic fracture network modeling for enhanced oil recovery, Circle Ridge Phosphoria/Tensleep reservoir, Wind River Reservation, Arapaho and Shoshone Tribes, Wyoming. U.S. Department of Energy, Tulsa, Oklahoma, 106 pp.
Leckenby, R.J., Sanderson, D.J., Lonergan, L., 2005. Estimating flow heterogeneity in natural fracture systems. Journal of Volcanology and Geothermal Research 148, 1–2. 116-129.
Liu, E., 2005. Effects of fracture aperture and roughness on hydraulic and mechanical properties of rocks: implication of seismic characterization of fractured reservoirs. Journal of Geophysics and Engineering 2 (1), 38–47.
Liu, L., 2006. Fracture characterization using borehole radar: Numerical modeling. Water, Air, and Soil Pollution: Focus 6 (1-2), 17–34.
Loiseau, P., 1987. Correlations between parameters. In: Bear, J., Tsang, C.F., de Marsily, G. (Eds.), Flow and Contaminant Transport in Fractured Rock. Academic Press.
Long, J.C.S. (Ed.), 1996. Rock Fractures and Fluid Flow: Contemporary Understanding and Applications. National Academy Press, Washington DC, 551 pp.
Malamud, B.D., Turcotte, D.L., 1999. Self-affine time series: measures of weak and strong persistence. Journal of Statistical Planning and Inference 80, 173–196.
Mandelbrot, B.B., 1983. The Fractal Geometry of Nature. W.H. Freeman and Co., New York, 480 pp.
Mandelbrot, B.B., 1985. Self-affine fractal dimension. Physica Scripta 32, 257–260.
Maros, Gy., Pásztor, Sz, 2001. New and oriented core evaluation method: ImaGeo. European Geologist 12, 40–43.
Maros, Gy., Koroknai, B., Palotás, K., Fodor, L., Dudko, A., Forián-Szabó, M., Zilahi-Sebess, L., Bán-György, E., 2004. Tectonic analysis and structural evolution of the north-eastern Mórágy Block. Annual Report of the Geological Institute of Hungary 2003, 371–386.
Marsan, D., Bean, C.J., 1999. Multiscaling nature of sonic velocities and lithology in the upper crystalline crust. Geophysical Research Letters 26, 275–278.
Matsumoto, N., Yomogida, K., Honda, S., 1992. Fractal analysis of fault systems in Japan and the Philippines. Geophysical Research Letters 19 (4), 357–360.
Mauldon, M., Derschowitz, B., in press. Fracture abundance measures: density, intensity and porosity. International Journal of Rock Mechanics and Mining Sciences.
McDermott, C.I., Sauter, M., Liedl, R., 2003. New experimental techniques for pneumatic tomographical determination of the flow and transport parameters of highly fractured porous rock samples. Journal of Hydrology 278, 1–4. 51-63.
Min, K.B., Jing, L., Stephansson, O., 2004. Determining the equivalent permeability tensor for fractured rock masses using stochastic REV approach: Method and application to the field data from Sellafield, UK. Hydrogeology Journal 12, 497–510.
Montemagno, C.D., Pyrak-Nolte, L.J., 1995. Porosity of natural fracture networks. Journal of Geophysical Research Letters 22, 1397–1400.
Neuzil, C.E., Tracy, J.V., 1981. Flow through fractures. Water Resources Research 17 (1), 191–199.
Onishi, C.T., Shimizu, I., 2003. Imaging of microcracks in granite by a fluorescent method assisted by laser scanning microscope, LSM. The Journal of Geological Society of Japan 109, 607–610.
Opheim, J.A., Gudmundsson, A., 1989. Formation and geometry of fractures, and related volcanism, of the Krafla fissure swarm, northeast Iceland. Bulletin of the Geological Society of America 101, 1608–1622.
Ortega, O.J., Marrett, R.A., Laubach, S.E., 2006. A scale-independent approach to fracture intensity and average spacing measurement. AAPG Bulletin 90 (2), 193–208.
Ouillon, G., Castaing, C., Sornette, D., 1996. Hierarchical geometry of faulting. Journal of Geophysical Research 101, 5477–5487.
Paillet, F.L., Kay, R.T., Yeskis, D., Pedler, W., 1993. Integrating well logs into a multi-scale investigation of a fractured sedimentary aquifer. The Log Analyst 34 (1), 13–23.
Pollard, D.D., Segall, P., 1987. Theoretical displacements and stresses near fractures in rock: with application to faults, joints, veins, dikes and solution surfaces. In: Atkinson, B. (Ed.), Fracture Mechanics of Rock. Academic Press, London.
Priest, S.D., Hudson, J., 1981. Estimation of discontinuity spacing and trace length using scanline surveys. International Journal of Rock Mechanics and Mineral Science 18, 183–197.
Priest, S.D., 2004. Determination of discontinuity size distribution from scanline data. Rock Mechanics and Rock Engineering 37 (5), 347–368.
Roberts, S., Sanderson, D.J., Gumiel, P., 1998. Fractal analysis of the Sn–W mineralization from central Iberia: Insights into the role of fracture connectivity in the formation of an ore deposit. Economic Geology 93, 360–365.
Segall, S.W., Pollard, D.D., 1983. Joint formation in granitic rocks of the Sierra Nevada. GSA Bulletin 94, 563–575.
Smirnova, N., Hayakawa, M., Gotoh, K., Volobuev, D., 2001. Scaling characteristics of ULF geomagnetic fields at the Guam seismoactive area and their dynamics in relation to the earthquake. Natural Hazards and Earth System Sciences 1, 119–126.
Telesca, L., Lapenna, V., Macchiato, M., 2004. Mono- and multi-fractal investigation of scaling properties in temporal patterns of seismic sequences. Chaos. Solitons and Fractals 19, 1–15.
Tezuka, K, Watanabe, K., 2000. Fracture network modelling of Hijiori hot dry rock reservoir by deterministic and stochastic crack network simulator, D/SC). Proceedings World Geothermal Congress, pp. 3933–3938.
Tóth, T.M., Hollós, Cs., Szűcs, É., Schubert, F., 2004. Conceptual fracture network model of the crystalline basement of the Szeghalom Dome, Pannonian Basin, SE Hungary. Acta Geologica Hungarica 47 (1), 19–34.
Tóth, T.M., 2004. Adatbázis repedéshálózat fraktál geometriai alapú szimulációjához a Bátaapáti kutatási területen mélyült mélyfúrások alapján, Database for fractal geometry-based fracture network simulation using wells representing the Bátaapáti field. In Hungarian. RHK KHT, 1–13.
Tsuchiya, N., Nakatsuka, K., 1995. A two-dimensional mono-fractal approach to natural fracture networks in rock. Geothermal Science and Technology 6, 63–82.
Turcotte, D.L., 1992. Fractals and Chaos in Geology and Geophysics. Cambridge University Press.
Twiss, R.J., Moores, E., 1992. Structural Geology. W.H. Freeman, 532 pp.
Vermilye, J.M., Scholz, C.H., 1995. Relation between vein length and aperture. Journal of Structural Geology 17 (3), 423–434.
Wanliss, J.A., Cersosimo, D.O., 2006. Scaling properties of high latitude magnetic field data during different magnetospheric conditions. International Conference on Substorms 8, 325–329.
Weiss, J., 2001. Fracture and fragmentation of ice: a fractal analysis of scale invariance. Engineering Fracture Mechanics 68 (17-18), 1975–2012.
Wildenschild, D., Hopmans, J.W., Vaz, C.M.P., Rivers, M.L., Rikard, D., Christensen, B.S.B., 2002. Using X-ray computed tomography in hydrology: systems, resolutions, and limitations. Journal of Hydrology 267, 285–297.
Witherspoon, P.A., Wang, J.S.Y., Iwai, K., Gale, J.E., 1980. Validity of cubic law for fluid flow in deformable rock fracture. Water Resources Research 16 (6), 1016–1024.
Yang, H.S., Kang, J.G., Kim, K.S., Kim, C.S., 2004. Groundwater flow characterization in the vicinity of the underground caverns in fractured rock masses by numerical modelling. Geosciences Journal 8 (4), 401–413.
Yielding, G., Walsh, J.J., Watterson, J., 1992. The prediction of small scale faulting in reservoirs. First Break 10, 449–460.
Zhang, L., Einstein, H.H., 1998. Estimating the mean trace length of rock discontinuities. Rock Mechanics and Rock Engineering 31 (4), 217–235.
Zhang, X., Sanderson, D.J., 2002. Numerical Modelling and Analysis of Fluid Flow and Deformation of Fractured Rock Masses. Pergamon, 288 pp.
Zimmermann, G., Burkhardt, H., Engelhard, L., 2003. Scale Dependence of Hydraulic and Structural Parameters in the Crystalline Rock of the KTB. Pure and Applied Geophysics 160 (5-6), 1067–1085.
Zimmerman, R.W., Bodvarsson, S., 1996. Hydraulic conductivity of rock fractures. Transport in Porous Media 23 (1), 1–30.